Scientia Iranica B (2019) 26(1), 311–322

Sharif University of Technology
Scientia Iranica
Transactions B: Mechanical Engineering
http://scientiairanica.sharif.edu

Optimization of the aerodynamic configuration of a tubular projectile based on blind kriging

Q. Zhao, Z.H. Chen*, Z.G. Huang, H.H. Zhang, and J. Ma[1]

National Key Laboratory of Transient Physics, Nanjing University of Science and Technology, Nanjing 210094, Jiangsu, China.

Received 7 December 2016; received in revised form 2 August 2017; accepted 25 December 2017

KEYWORDS
Tubular projectiles;
Blind kriging;
Aerodynamic configuration;
Optimal design;
Flow structure.

Abstract. Based on optimal Latin hypercube design of computer experiments, blind kriging surrogate model, and sequential quadratic programming method, the optimal design of the aerodynamic configuration of a 30 mm tubular projectile is carried out through commercial software products such as UG, ICEM CFD, FLUENT, etc. The aerodynamic configuration has been optimized to minimize the drag coefficients at different Mach numbers and maximize the kinetic energies at given flight ranges. The optimal configuration is obtained and discussed. Finally, the similarities and differences of the flow structure and aerodynamic characteristics between the original and optimal tubular projectiles are compared. The numerical optimal method proposed in this paper for optimizing the tubular projectile can provide important guidances for the aerodynamic configuration design of projectiles.

1. Introduction

Tubular projectiles, also known as hollow projectiles, are virtually thin-walled tubes with beveled ends. Compared with conventional solid projectile, the tubular projectile has many advantages [1,2]: small drag, high accuracy and precision, low cost, and small recoil force. The tubular projectile has broad application background in the ammunition field of air defense, and it has been proved very promising. Therefore, studying the optimal design of the tubular projectile configuration is quite necessary.

The study of tubular projectile has attracted much attention for many years due to its superiority, mainly focusing on its applications [3,4] and wind tunnel tests [5,6]. With the rapid improvement of computer capacity and the development of Computational Fluid Dynamics (CFD) in recent years, many studies have focused on numerical simulation of the flow field around the tubular projectile [7,8], and the flow structure and aerodynamic characteristics are studied. Our research group has also done a lot of work from numerical simulation to numerical optimization of the tubular projectile [1,2]. Li and Chen [2] dedicatedly studied the aerodynamic characteristics of the tubular projectile under real conditions with the use of FLUENT. Based on numerical simulations of the two-dimensional flow fields around different configurations at Mach number of 3.0, Huang et al. [1] optimized the aerodynamic configuration of a simplified tubular projectile using the exhaustive method and obtained the optimal configuration with minimum drag coefficient. However, it appears that the exhaustive method is appropriate based on the extremely limited number of design variables.

This paper presents an approach to the optimal design of supersonic tubular projectiles based on

1. *Present address: School of Mechanical and Power Engineering, Nanjing Tech University, Nanjing 211816, Jiangsu, China.*
*. *Corresponding author. Tel.: +86 25 84303929*
E-mail address: chenzh@njust.edu.cn (Z.H. Chen)

doi: 10.24200/sci.2017.20015

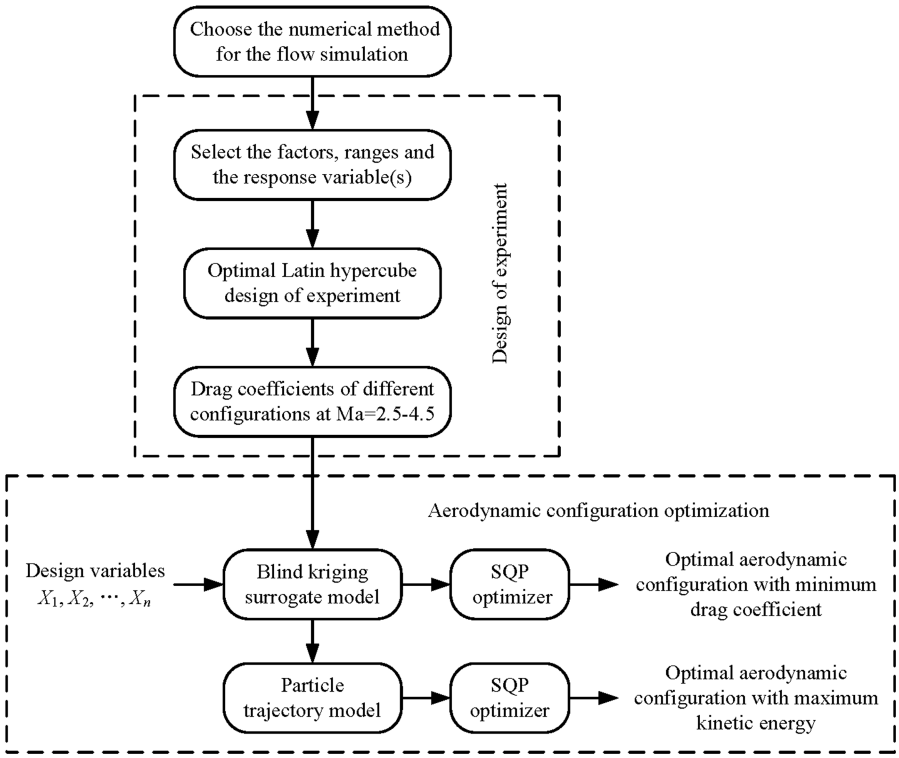

Figure 1. Flowchart of the optimization process of aerodynamic configuration.

blind kriging surrogate model. Up to now, surrogate model has been successfully applied to the aerodynamic configuration optimization of airfoils [9], rockets [10], guided projectiles [11], and missiles [12]. As a typical surrogate model, kriging is widely used [13-15]. Blind kriging is the extension of kriging whose predictor is more complicated and more robust, and it has been successfully applied to many different kinds of optimization problems [16].

In this paper, numerical simulations are performed for a 55.09 mm tubular projectile, and the drag coefficients at Mach number of 2.3-4.5 are obtained. Simultaneously, the computational predictions are compared with the free-flight results. Based on blind kriging surrogate model, conducting research on the optimal design of the aerodynamic configuration of our previously studied 30 mm tubular projectile is then carried out using the Sequential Quadratic Programming (SQP) method.

2. Optimization process of the aerodynamic configuration of supersonic tubular projectiles

Surrogate-based optimization approach, which has recently attracted much attention due to the ability of substantially reducing the computational cost, has proven quite useful for engineering design problems. The actual process of aerodynamic configuration optimization based on surrogate model is shown in Figure 1, and it involves the following four primary steps:

1. Choose the numerical method for the flow simulation;
2. Design computational experiments for a collection of pairs of inputs and responses for use;
3. Build blind kriging surrogate models with high accuracy;
4. Conduct an optimization search based on the surrogate models.

In this paper, the original 30 mm tubular projectile is chosen as an optimization object. First, the same numerical method used in [1] is selected for the flow simulation of the tubular projectile. Then, a computational experiment is conducted using the optimal Latin hypercube design, and the drag coefficients of a few selected tubular projectile configurations at different Mach numbers are obtained. Afterwards, blind kriging surrogate models are built for the drag coefficients at different Mach numbers. Finally, the SQP is selected as a method for the optimal design of the configuration of a supersonic tubular projectile. The following sections provide a detailed process of each step.

2.1. Computational method

Considering that the supersonic tubular projectile is mainly used for air defense, it must make full use of

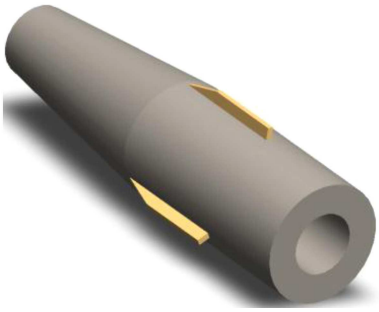

Figure 2. The tubular projectile model from [6].

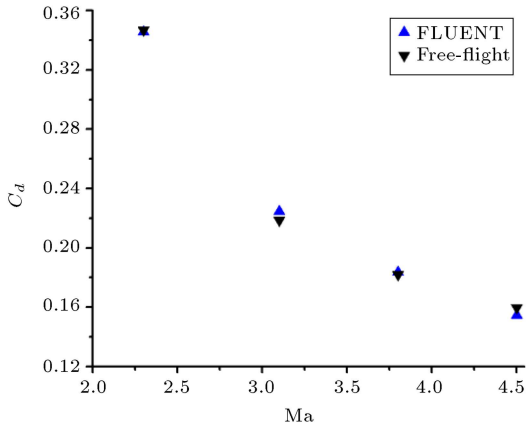

Figure 3. Comparison of the drag coefficients at different Mach numbers.

the kinetic energy of the ascending stage. During the ascending stage, the tubular projectile almost flies with zero angle of attack; hence, the zero attack-angle flight model reflects the practical flight of a tubular projectile within the effective range. Therefore, the zero angle of attack is used in our calculation model during the simulation process.

The same numerical method is chosen, as used in [1]. The compressible Navier-Stokes equations and the Spalart-Allmaras turbulence modeling are adopted. The convection term and viscosity term are discretized by the second-order Advection Upstream Splitting Method (AUSM) scheme and second-order central difference scheme, respectively. In addition, the second-order Runge-Kutta scheme is used for time stepping. In order to validate the above method, a tubular projectile [6], shown in Figure 2, is taken as an example. The drag coefficient results of CFD and free flight at Mach number of 2.3-4.5 are shown in Figure 3. As illustrated, our numerical results agree well with free-flight results of [6].

Our previously studied 30 mm tubular projectile with a length-to-diameter ratio of 2.7 is selected as the original model, and its two-dimensional model is shown in Figure 4. The tubular projectile is composed of the nose, the cylindrical body, the boattail, and the internal part. The internal part is a tube that consists

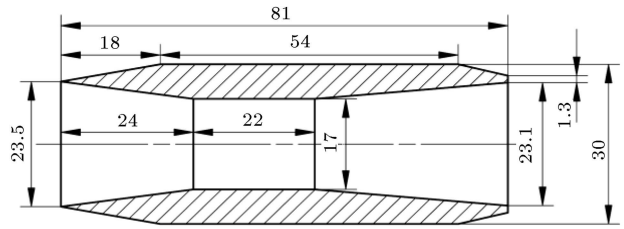

Figure 4. The original two-dimensional tubular projectile (unit: mm).

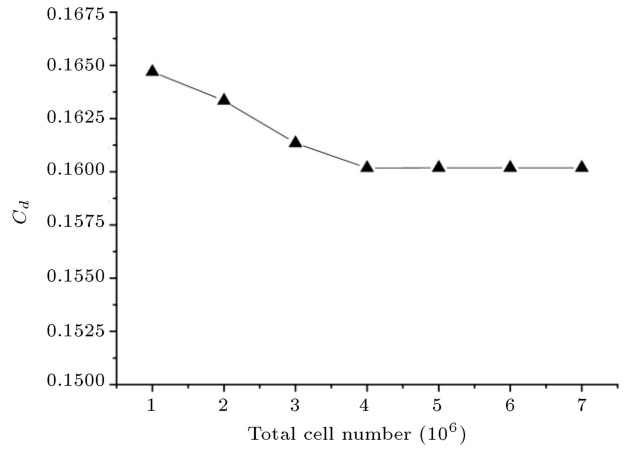

Figure 5. The change of the drag coefficient according to the total cell number at Ma = 3.0.

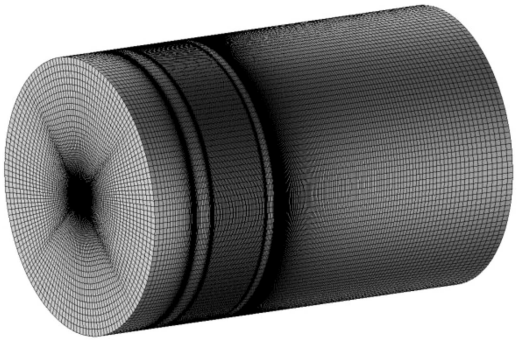

Figure 6. The computational domain size and the final mesh of the tubular projectile.

of the convergence section, the cylinder tube, and the divergence section. The computational domain is taken as a cylinder topology, and the tubular projectile is placed at the center of the symmetry plane. The diameter and depth of the cylinder are $8D$ and $12D$, respectively, and D is the diameter of the tubular projectile. The computational mesh is generated by the mesh generation software, i.e., ICEM CFD. Moreover, by considering the particular structure of the tubular projectile, the O-grid generation technique is applied to generate three-dimensional body-fitted structured mesh. After repeated calculations and the convergence test at Ma = 3.0 shown in Figure 5, about 4 million mesh cells in computational domain are selected. Figures 6-8 show the computational domain size and the

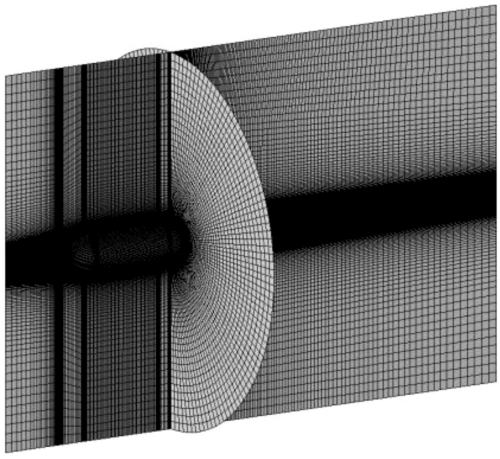

Figure 7. The surface and sectional meshes of the tubular projectile.

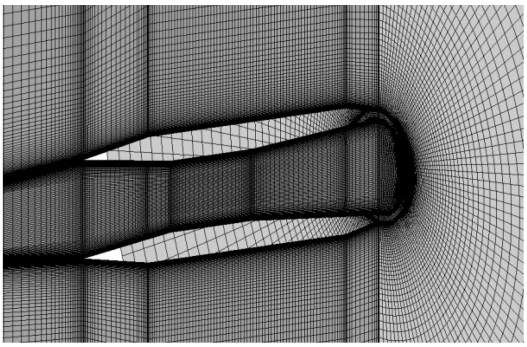

Figure 8. The mesh around the tubular projectile.

final mesh, the surface and sectional meshes, and the mesh around the tubular projectile, respectively. As for the boundary conditions, the no-slip wall condition and pressure far-field condition are used for the projectile surface and flow inlet and exit, respectively. The first layer distance from the wall is selected to maintain the y^+ value in the range of 30-60 for all the cases at different Mach numbers. Taking Ma = 3.0 as an example, the first layer distances from the inner and external walls are 1.7×10^{-5} m and 2.0×10^{-5} m, respectively, and the range of y^+ values is 31.62-57.81.

2.2. Design of computational experiments

Design Of Experiments (DOE), also known as sampling, is a collection of pairs of inputs and responses from runs of a computer model, and it has a significant impact on the accuracy of a surrogate model. The actual process of the DOE involves intelligent selection of sample points in the design space. A great variety of methods exist for this purpose, such as the full factorial design [17], the fractional factorial design [17], the Latin Hypercube Design (LHD) [18], and the Optimal Latin Hypercube Design (OLHD) [19].

The LHD and OLHD are just two of the most common methods for designing computer experiments. The OLHD is an improvement of the LHD. Mckay et al. [18] proposed LHD. Consider the case where we wish to sample M points in the n-dimensional vector space. The LHD strategy is as follows:

1. Divide the range of each dimension into M intervals with equal marginal probability;
2. Sample once from the intervals in each dimension and pair them at random.

Because the sample points obtained using LHD are made of combinations of each dimension randomly, the potential lack of uniformity is unavoidable. To improve the uniformity, the enhanced stochastic evolutionary algorithm and efficient methods for evaluating optimality criterion are developed [19]. This computer experiment strategy is the so-called OLHD adopted in this paper. It has been proved that the OLHD offers a substantial improvement over the LHD on the uniformity and maintains good computational efficiency in sampling. Furthermore, we can easily determine the sample size according to the prediction accuracy of a surrogate model in an OLHD. Thus the method of OLHD is chosen for DOE. By considering the trade-off between computational complexity and prediction accuracy of a surrogate model, the sample size of 35 is finally determined.

Generation of an OLHD for the design variables, $\mathbf{X} = \{X_1, X_2 \cdots, X_n\}$, produces a set of M vectors of length n. Then, commercial software products, such as UG, ICEM CFD, and FLUENT, are used to calculate the drag coefficient of each configuration. The flowchart of the DOE process is shown in Figure 9, and the detailed process is as follows:

1. Choose the numerical experiment method, OLHD, and design numerical experiment;
2. Update configuration i as well as output the mass of the tubular projectile through a C++ program, which is developed on the UG platform;
3. Run the file ICEM_CFD.rpl which contains a record of the commands used to generate the computational structured mesh automatically via a script;
4. Run the file FLUENT.jou which contains a sequence of FLUENT commands via a script and obtain the corresponding drag coefficient;
5. Return to steps 2-4 until i reaches sample size M.

2.3. Blind kriging surrogate model

A wide variety of approaches can be used to construct a surrogate model, including polynomial regression, kriging, support vector regression, and radial basis functions. Kriging is of particular popularity for approximating deterministic computer experiments, and it is widely used for obtaining a surrogate model. Blind kriging, proposed by Joseph et al. [16], extends kriging with a Bayesian feature selection method. The

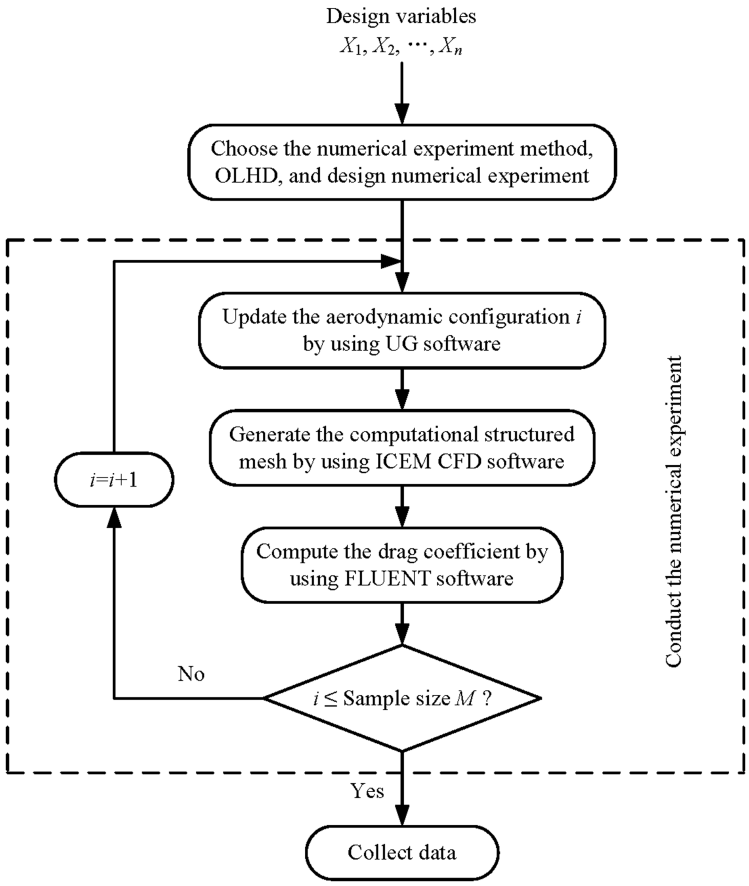

Figure 9. Flowchart of the DOE process.

mathematical formula of blind kriging is given as follows:

$$Y(\mathbf{x}) = \mu(\mathbf{x}) + Z(\mathbf{x}), \tag{1}$$

where $\mu(\mathbf{x}) = \sum_{i=0}^{m} \mu_i v_i(\mathbf{x})$ is a trend function, and $Z(\mathbf{x})$ is a stochastic process with mean 0 and variance σ_m^2. In addition, $v_i(\mathbf{x})$, μ_i, and m are the basis function, the corresponding coefficient, and the number of basis functions, respectively.

Consider predicted value $\hat{y}(\mathbf{x})$ at a new point $\mathbf{x}$ by a linear model:

$$\hat{y}(\mathbf{x}) = \sum_{i=0}^{m} \mu_i v_i + \sum_{i=0}^{t} \beta_i u_i, \tag{2}$$

where u_i denotes the candidate function, and t is the number of candidate functions. As for $\sum_{i=0}^{t} \beta_i u_i$, it includes the linear effects, quadratic effects, and two-factor interactions. The linear effects and quadratic effects are defined, respectively, as follows:

$$x_{jl} = \frac{\sqrt{3}}{\sqrt{2}}(x_j - 2), \tag{3}$$

$$x_{jq} = \frac{1}{\sqrt{2}}(3(x_j - 2)^2 - 2), \tag{4}$$

where $j = 1, 2, \cdots, p$, and p denotes the number of input dimensions. Taking a two-dimensional input $\mathbf{x}^T = (x_1, x_2)$ as an example, from Eq. (2), we get the expression for $\hat{y}(\mathbf{x})$, $\sum_{i=0}^{m} \mu_i v_i + \sum_{i=0}^{8} \beta_i u_i$, where $u_0 = 1$, $u_1 = x_{1l}$, $u_2 = x_{1q}$, $u_3 = x_{2l}$, $u_4 = x_{2q}$, $u_5 = x_{1l}x_{2l}$, $u_6 = x_{1l}x_{2q}$, $u_7 = x_{1q}x_{2l}$, and $u_8 = x_{1q}x_{2q}$.

Considering the fact that the number of sample points available may be less than the number of candidate functions, a frequentist estimation of $\boldsymbol{\beta} = (\beta_0, \beta_1, \cdots, \beta_t)^T$ becomes impossible; therefore, a prior distribution is postulated for $\boldsymbol{\beta}$:

$$\boldsymbol{\beta} \sim N(\mathbf{0}, \tau_m^2 \mathbf{R}), \tag{5}$$

where $\mathbf{0}$ is a vector of length $t+1$, and $\mathbf{R}$ is a $(t+1) \times (t+1)$ diagonal matrix.

Define vectors $\mathbf{l}_i$ and $\mathbf{q}_i$ with the following properties:

1. If β_i includes the linear effect of factor j, $l_{ij} = 1$; otherwise, $l_{ij} = 0$;
2. If β_i includes the quadratic effect of factor j, $q_{ij} = 1$; otherwise, $q_{ij} = 0$.

Then, diagonal matrix $\mathbf{R}$ can be expressed as follows:

$$\mathbf{R}=\begin{bmatrix}\mathbf{r}_l^{l_1}\cdot\mathbf{r}_q^{q_1} & 0 & \cdots & 0\\ 0 & \ddots & 0 & \vdots\\ \vdots & 0 & \ddots & 0\\ 0 & \cdots & 0 & \mathbf{r}_l^{l_{t+1}}\cdot\mathbf{r}_q^{q_{t+1}}\end{bmatrix}, \tag{6}$$

where:

$$\mathbf{r}_l=\frac{3-3\psi(2)}{3+4\psi(1)+2\psi(2)}, \tag{7}$$

$$\mathbf{r}_q=\frac{3-4\psi(1)+\psi(2)}{3+4\psi(1)+2\psi(2)}. \tag{8}$$

Subsequently, the posterior mean of $\boldsymbol{\beta}$ is derived as follows:

$$\hat{\boldsymbol{\beta}}=\frac{\tau_m^2}{\sigma_m^2}\mathbf{R}\mathbf{U}^T\boldsymbol{\psi}^{-1}(\mathbf{y}-\mathbf{v}_m\hat{\boldsymbol{\mu}}_m), \tag{9}$$

where $\mathbf{U}$ is the model matrix of all candidate variables, $\boldsymbol{\psi}$ is the correlation matrix of the sample points, and $\mathbf{v}_m$ is the model matrix of currently chosen candidate variables. The larger the absolute coefficient $|\beta_i|$ is, the more important the candidate variable is. Thus, the candidate variable with the largest $|\beta_i|$ will be selected in each step $m=0,1,2\cdots$. The best value of m is chosen using Cross-Validation Prediction Error (CVPE), which is defined as follows:

$$CVPE(m)=\sqrt{\frac{1}{M}\sum_{i=1}^{M}(y_i(\mathbf{x})-\hat{y}_i(\mathbf{x}))^2}, \tag{10}$$

where $\hat{y}_i(\mathbf{x})$ is the predicted value after removing the ith sample point, $y_i(\mathbf{x})$ denotes the corresponding actual value, and M is the number of sample points. Then, m with minimum $CVPE(m)$ is chosen as the best value. Subsequently, the current best set of features is chosen to construct the final blind kriging.

2.4. SQP method

The SQP is selected as the method of trajectory optimization. The SQP represents the state of the art in nonlinear programming methods, with advantages such as fast convergence and high precision; in addition, it is one of the most effective methods available for trajectory optimization [20]. The basic idea of SQP is to model the nonlinear programming problems for a given iteration, by a Quadratic Programming (QP) subproblem, and then the solution is used to construct this subproblem to obtain a better approximation of the solution. This process is conducted iteratively until a converged solution is obtained.

The constrained nonlinear programming problem has the following form:

$$\left.\begin{array}{ll}\min f(\mathbf{x}) & \\ g_i(\mathbf{x})=0, & i=1,2,\cdots,n_e\\ g_i(\mathbf{x})\le 0, & i=n_e+1,\cdots,n_t\end{array}\right\}, \tag{11}$$

where $f(\mathbf{x})$ is the objective function, $g_i(\mathbf{x})$ is the linear or nonlinear function; $g_i(\mathbf{x})$ denotes an equality constraint for $i=1\sim n_e$, while, for $i=n_e+1\sim n_t$, $g_i(\mathbf{x})$ denotes the inequality constraint.

After linearizing the nonlinear constraints, the following form of subproblem QP can be obtained:

$$\left.\begin{array}{ll}\min & \frac{1}{2}\mathbf{d}^T\mathbf{B}^{(k)}\mathbf{d}+(\nabla f(\mathbf{x}^{(k)}))^T\mathbf{d}\\ \left[\nabla g_i(\mathbf{x}^{(k)})\right]^T\mathbf{d}+g_i(\mathbf{x}^{(k)})=0, & i=1,2,\cdots,n_e\\ \left[\nabla g_i(\mathbf{x}^{(k)})\right]^T\mathbf{d}+g_i(\mathbf{x}^{(k)})\le 0, & i=n_e+1,\cdots,n_t\end{array}\right\}, \tag{12}$$

where $\mathbf{d}$ is the search direction, $\nabla f(\mathbf{x}^{(k)})$ is the gradient of the objective function at the current iterate $\mathbf{x}^{(k)}$, $\mathbf{B}^{(k)}$ is a positive definite approximation of the Hessian matrix of the Lagrangian function updated by the Broyden-Fletcher-Goldfarb-Shanno (BFGS) algorithm. The QP subproblem can be solved through a quadratic approximation of the Lagrangian function:

$$L(\mathbf{x},\boldsymbol{\lambda})=f(\mathbf{x})+\sum_{i=1}^{n_t}\lambda_i g_i(\mathbf{x}), \tag{13}$$

where $\boldsymbol{\lambda}$ is the vector of Lagrange multipliers, and λ_i is the ith Lagrange multiplier.

The main steps of the SQP method can be summarized as follows [21]:

1. Give the first iterate, $\mathbf{x}^{(1)}$, a positive definite matrix $\mathbf{B}^{(1)}\in\mathbf{R}^{n\times n}$ (an identity matrix) and let $k=1$;
2. Compute search direction $\mathbf{d}^{(k)}$ and Lagrange multiplier $\boldsymbol{\lambda}^{(k+1)}$ by solving the QP subproblem (12);
3. Determine stepsize α_k by an appropriate line search procedure to obtain a sufficient decrease in a merit function and, then, obtain a new iterate, $\mathbf{x}^{(k+1)}$, as follows: $\mathbf{x}^{(k+1)}=\mathbf{x}^{(k)}+\alpha_k\mathbf{d}^{(k)}$;
4. Calculate the difference in $\mathbf{x}^{(k)}$ and obtain the difference $\|\Delta\mathbf{x}^{(k)}\|$ as follows: $\|\Delta\mathbf{x}^{(k)}\|=\|\alpha_k\mathbf{d}^{(k)}\|=\|\mathbf{x}^{(k+1)}-\mathbf{x}^{(k)}\|$. If $\|\Delta\mathbf{x}^{(k)}\|$ is sufficient small, then the iteration is over, otherwise return to step 5;
5. Update the positive definite matrix $\mathbf{B}^{(k)}$ to $\mathbf{B}^{(k+1)}$ by the BFGS algorithm and let $k=k+1$. Then, return to step 2.

3. Optimal design of a typical tubular projectile

Case studies seek to solve the problem of optimal design of the tubular projectile. Firstly, based on

blind kriging surrogate model, the configuration of the tubular projectile has been optimized for minimum drag coefficient using the SQP method. The minimum drag coefficient and optimal configuration parameters at Ma = 2.5 − 4.5 are obtained, respectively. Then, by applying the simple particle trajectory model [20], the configuration of the tubular projectile is optimized to maximize the kinetic energy in the given flight ranges through the SQP method, and the variation range of each configuration parameter is obtained. Finally, the similarities and differences of the flow structure and aerodynamic characteristics between the original and optimal tubular projectiles are compared.

3.1. Main design variables

Our previously numerical simulation shows that the ratio of the inner throat area to inlet area and effective Mach number essentially govern the flight condition of a specific tubular projectile. Since the throat and inlet diameters have been defined in the early design phase, they are not design variables. The design variables of a typical tubular projectile and their ranges are shown in Figure 10 and Table 1, respectively.

3.2. Minimization of the drag

Based on the software products, such as UG, ICEM CFD, FLUENT, etc., the whole calculation process is conducted automatically via scripting, and the drag coefficients corresponding to 35 numerical samples at Ma = 2.5, 3.0, 3.5, 4.0, and 4.5 are obtained, respectively. Then blind kriging surrogate model is established for the drag coefficients at different Mach numbers. As for the drag coefficient of a specific configuration at any Mach number within the range, it is obtained by using the Lagrange interpolation method.

In order to evaluate the prediction accuracy of the blind kriging surrogate model and Lagrange interpolation method, the Mean Absolute Percentage Error (MAPE) is used, defined as follows:

$$\text{MAPE} = \frac{1}{N}\sum_{i=1}^{N}\frac{|C_d - \hat{C}_d|}{C_d} \times 100\%, \tag{14}$$

where N is the number of testing samples, C_d and $\hat{C}_d$ are the actual numerical and predicted values of the drag coefficient, respectively. In this paper, eight testing samples are obtained using the OLHD, and the MAPE values at Ma = 2.5 − 4.5 are obtained and shown in Figure 11. It can be seen that the minimum and maximum MAPE values are 0.83% and 2.56%, respectively, indicating that both the blind kriging surrogate model and Lagrange interpolation method have good prediction accuracy.

Table 2 gives the optimal configuration parameters with minimum drag at Ma = 2.5 − 4.5. The value of the optimal configuration parameter, X_2, is the same at different Mach numbers. For optimal configuration parameters X_1, X_3, and X_4, their variation ranges are 44.16-46.65 mm, 40.37-45.00 mm, and 30.50-35.48 mm, respectively.

The comparison of the drag coefficients of the original and optimal tubular projectiles is shown in

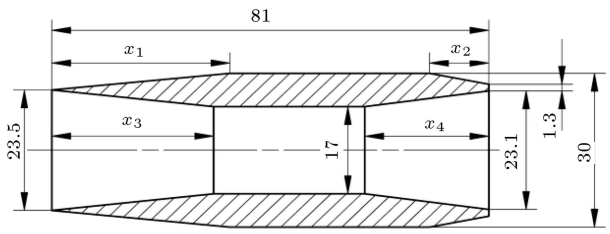

Figure 10. Schematic of design variables of a typical tubular projectile (unit: mm).

Table 1. Design variables and their ranges.

Variables	Lower bound (mm)	Upper bound (mm)
X_1	16.00	50.00
X_2	6.00	16.00
X_3	20.00	45.00
X_4	10.00	36.00

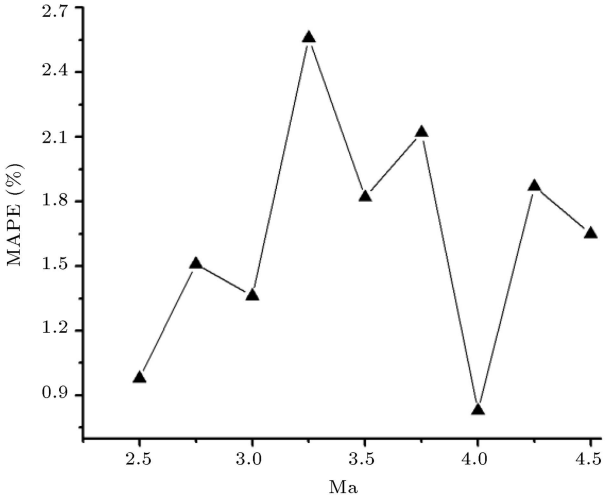

Figure 11. The MAPE values at different Mach numbers.

Table 2. The optimal configuration parameters with minimum drag.

Mach number	X_1 (mm)	X_2 (mm)	X_3 (mm)	X_4 (mm)
2.5	46.65	16.00	44.62	30.82
3.0	45.57	16.00	44.75	33.81
3.5	44.16	16.00	45.00	35.01
4.0	45.58	16.00	42.36	35.48
4.5	46.29	16.00	40.37	30.50

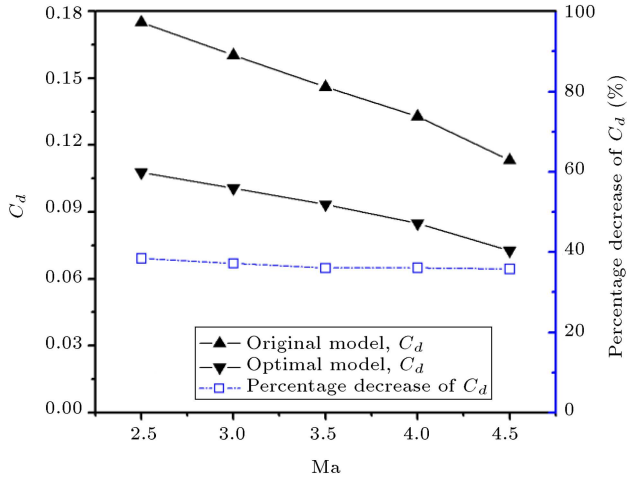

Figure 12. Comparison of the drag coefficients of two tubular projectiles at different Mach numbers.

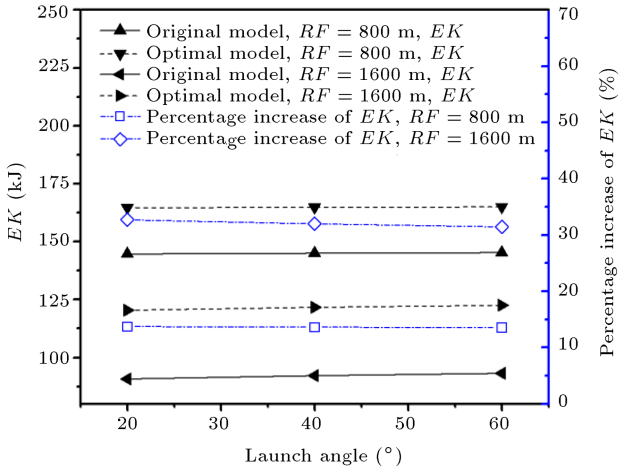

Figure 13. Comparison of the kinetic energies of two tubular projectiles at different launch angles.

Figure 12. Compared with the drag coefficient of the original tubular projectile at the same Mach number, the drag coefficient of the optimal tubular projectile is smaller, and the percentage decreases of the drag coefficients at Ma $= 2.5 - 4.5$ are all over 35.0%, indicating that the optimal results are satisfactory.

3.3. Maximization of the kinetic energy

Considering that the 30 mm tubular projectile is mainly used for short-range air defense, reaching a target with maximum kinetic energy is of vital importance. It is necessary to conduct an optimal design of the tubular projectile to maximize the kinetic energy at a given flight range. By applying the simple particle trajectory model, based on the blind kriging surrogate models established for the drag coefficients at Ma = 2.5-4.5 in Section 3.2, the configuration has been optimized for maximum kinetic energy in flight ranges of 800 m and 1600 m, respectively, and the results are shown in Table 3 and Figure 13, where RF denotes the flight range and EK denotes the kinetic energy. In addition, all of tubular projectiles have the same muzzle kinetic energy, $EK = 220$ kJ.

Table 3. The optimal configuration parameters with maximum kinetic energy in given flight ranges.

RF (m)	Launch angle (°)	X_1 (mm)	X_2 (mm)	X_3 (mm)	X_4 (mm)
800	20	42.22	14.71	40.02	31.17
	40	42.34	14.73	40.10	31.15
	60	42.41	14.74	40.08	31.18
1600	20	40.90	14.78	40.18	31.67
	40	40.96	14.77	40.13	31.66
	60	40.83	14.76	40.12	31.69

From Table 3, we can conclude that the variation ranges of optimal configuration parameters, X_1, X_2, X_3, and X_4, are 40.83-42.41 mm, 14.71-14.78 mm, 40.02-40.18 mm, and 31.15-31.69 mm, respectively. Figure 13 shows a comparison of the kinetic energies of end-points of both original and optimal tubular projectiles at different launch angles. As for the average kinetic energies of three different launch angles of the original and optimal tubular projectiles, their values are 145.03 kJ and 164.84 kJ as well as 92.07 kJ and 121.56 kJ in the given flight ranges of 800 m and 1600 m, respectively. Increase rates in the percentage of the kinetic energies of the optimal tubular projectile are respectively above 10% and 30% as compared with those of the original tubular projectile. The optimization results of the tubular projectile are satisfactory and greatly improve the aerodynamic performance of the original tubular projectile.

3.4. Comparison of aerodynamic characteristics

Taking the optimal configuration of the tubular projectile as an example for numerical simulation, it has the averaged optimized parameters of $X_1 = 40.90$ mm, $X_2 = 4.77$ mm, $X_3 = 40.14$ mm, and $X_4 = 31.67$ mm. The comparison of pressure contours of both original and optimal tubular projectiles at Ma = 2.5, 3.5, and 4.5 is shown in Figures 14-16.

From Figures 14-16, despite different configurations, the flow fields around the two tubular projectiles are symmetrical, and the main flow structures are the same. As for the external flow, the oblique shock and expansion waves are generated at the nose tip and the boattail, respectively. Behind the expansion waves, the pressure decreases sharply. Compared with the external flow, the internal flow is more complicated. The oblique shock waves interact with each other and reflect off the corresponding inner walls, which

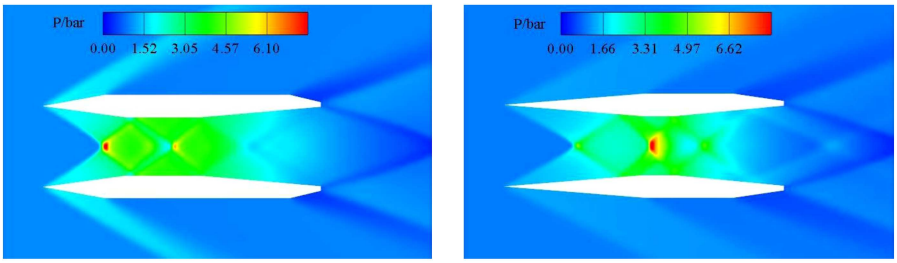

(a) Original projectile (b) Optimal projectile

Figure 14. The pressure contours of two tubular projectiles at Ma = 2.50.

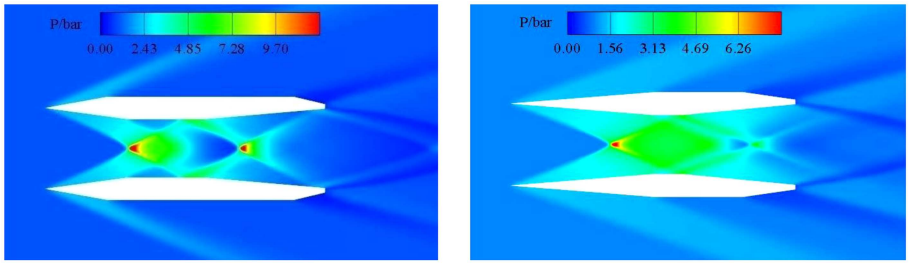

(a) Original projectile (b) Optimal projectile

Figure 15. The pressure contours of two tubular projectiles at Ma = 3.50.

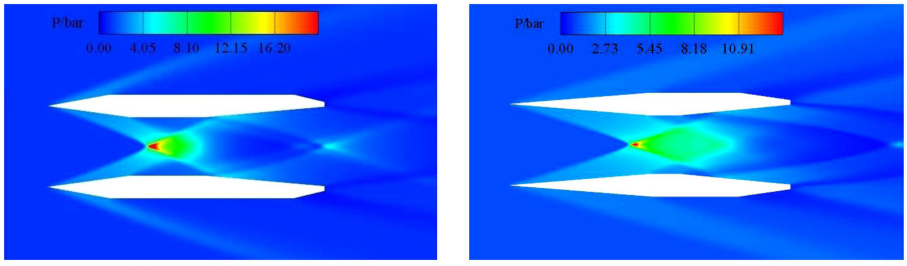

(a) Original projectile (b) Optimal projectile

Figure 16. The pressure contours of two tubular projectiles at Ma = 4.50.

generates a series of similar structures of oblique and reflected shock waves. The highest pressures around two tubular projectiles all occur in internal flows.

Despite the above-described similarities, there are some obvious differences between the two tubular projectiles. On the one hand, the intensity of oblique shock waves of the optimal one is weaker than that of the original one at the same Mach number. Then, the external wall pressure around the optimal tubular projectile is much smaller than that around the original one; hence, the optimal tubular projectile has smaller external wall drag. In addition, the location and pressure of the first intersection point of oblique shock waves are different. The location of the optimal one is farther from the nose tip, and its value of pressure is also smaller. However, for Ma = 2.5, the pressure of the second intersection point of oblique shock waves of the optimal one is a slightly higher than the internal pressure of the original one.

Flow structures of the two tubular projectiles also vary with Mach number. According to Figures 14-16, it is observed that the higher the Mach number, the smaller the oblique angle of shock wave at the nose, and the pressure shows an opposite trend. In addition, the first intersection point of oblique shock waves moves toward the boattail with the increase of Mach number.

The total drag coefficients of both original and optimal tubular projectiles at different Mach numbers are shown in Figure 17. As observed, C_d of both original and optimal tubular projectiles decreases with the increase of Mach number for supersonic flow, which agrees well with the variation of normal projectiles. The value of C_d of the optimal tubular projectile is much smaller, and its decrease percentage at Ma = 2.5-4.5 is above 29%.

The comparison of drag coefficients of each portion of two tubular projectiles is presented in Figures 18-20, where C_{de}, C_{di}, and C_{db} denote the external wall, inner wall, and base drag coefficients, respectively. The external wall drag accounts for the most of the total drag, approximately 60-70%. The inner wall drag is comparatively lower, and the base drag is the least. Therefore, the optimization of external configuration mainly causes the decrease of the total drag. Both C_{de}

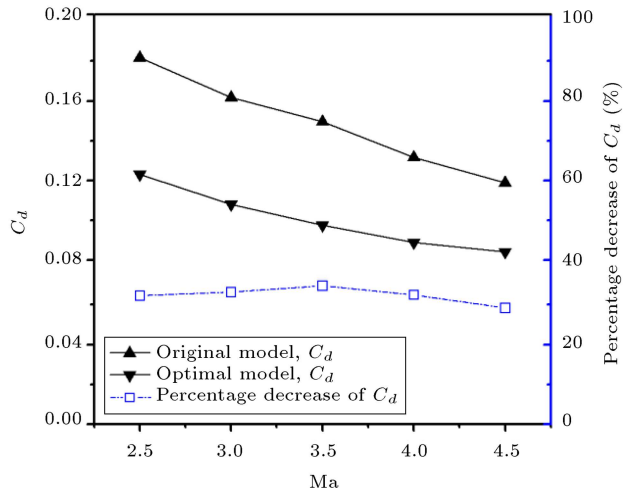

Figure 17. Comparison of total drag coefficients of two tubular projectiles.

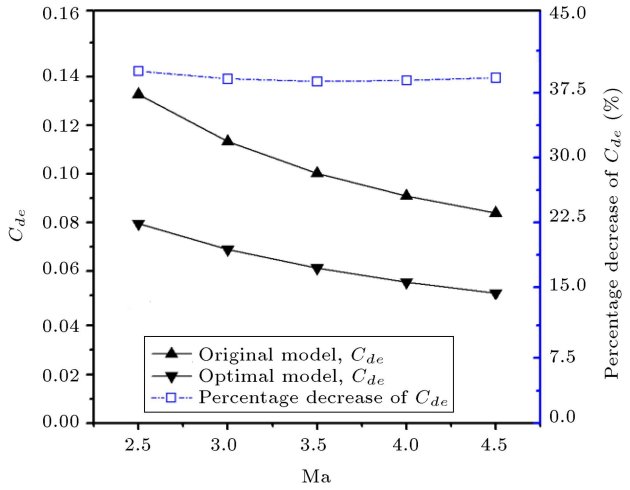

Figure 18. Comparison of the external wall drag coefficients of two tubular projectiles.

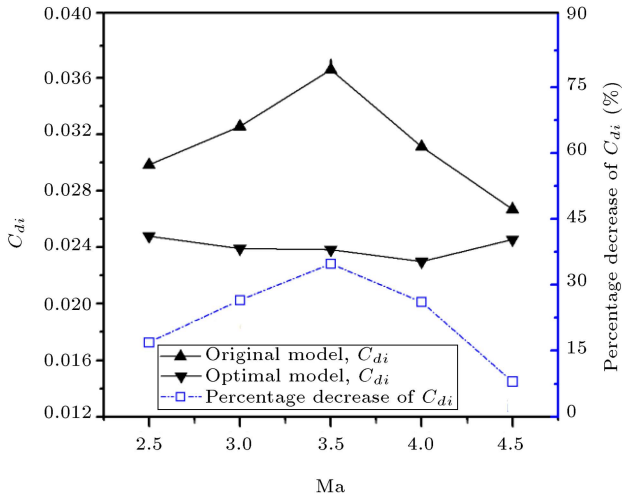

Figure 19. Comparison of the inner wall drag coefficients of two tubular projectiles.

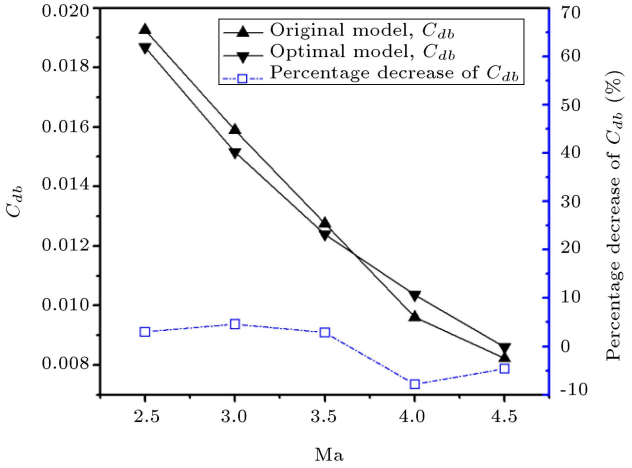

Figure 20. Comparison of the base drag coefficients of two tubular projectiles.

and C_{db} of the two tubular projectiles decrease with the increase of Mach number, while it is not the same for C_{di} due to the complexity of the internal flow.

4. Conclusions

A method for aerodynamic configuration optimization of a supersonic tubular projectile using DOE and surrogate model was proposed and validated in this paper. The whole process of the DOE was conducted automatically with the use of commercial software products, such as UG, ICEM CFD, and FLUENT. The method incorporates a SQP algorithm that, when coupled to the blind kriging surrogate model, produces an optimal configuration design of the tubular projectile with respect to the objectives of minimum drag coefficient and maximum kinetic energy.

The optimal design of our previously studied 30 mm tubular projectile is taken as an example. The computational results show that optimal aerodynamic configurations with minimum drag coefficient are different at different Mach numbers; however, the variations of the configurations are small. This changing trend is also true for optimal aerodynamic configurations with maximum kinetic energy in different flight ranges. Meanwhile, the comparison of drag coefficients of each portion of the original and optimal tubular projectiles was made, and the optimization of the external configuration was mainly the cause of total drag decrease. The method proposed in this paper can provide important guidances for the aerodynamic configuration design of projectiles.

Acknowledgements

This work is supported by Postgraduate Research & Practice Innovation Program of Jiangsu Province (No. KYCX17_0392) and Natural Science Foundation of

Shanghai (No. 17ZR1430100). The authors also thank the anonymous referees of this paper for their kind comments and suggestions, which are all valuable and very helpful for revising and improving our paper.

Nomenclature

$\mathbf{B}^{(k)}$	Positive definite matrix
C_d	Drag coefficient
$\hat{C}_d$	Predicted drag coefficient
C_{db}	Base drag coefficient
C_{de}	External wall drag coefficient
C_{di}	Inner wall drag coefficient
$\mathbf{d}$	Search direction
EK	Kinetic energy (kJ)
$f(\mathbf{x})$	Objective function
$g_i(\mathbf{x})$	Linear or nonlinear function
$\mathbf{l}_i$	Indicator vector for linear term
m	Number of basis functions
M	Size of the sample
n_e	Number of equality constraints
n_t	Number of equality and inequality constraints
N	Number of testing sample
p	Number of input dimensions
$\mathbf{q}_i$	Indicator vector for quadratic term
$\mathbf{R}$	Diagonal matrix
RF	Flight range (m)
t	Number of candidate functions
u_i	ith candidate function
$\mathbf{U}$	Model matrix of all candidate variables
$v_i(\mathbf{x})$	ith basis function
$\mathbf{v}_m$	Model matrix of currently chosen candidate variables
$\mathbf{x}$	Vector of design variables
$\mathbf{x}^{(k)}$	Current iterate
$\Delta\mathbf{x}^{(k)}$	Difference in $\mathbf{x}^{(k)}$
x_{jl}	Linear component of the jth factor
x_{jq}	Quadratic component of the jth factor
$\mathbf{y}$	Data vector
$y_i(\mathbf{x})$	Actual value after removing the ith sample point
$\hat{y}_i(\mathbf{x})$	Predicted value at after removing the ith sample point
$Z(\mathbf{x})$	Stochastic process
α_k	Positive scalar stepsize
$\boldsymbol{\beta}$	Vector containing $\beta_0, \cdots, \beta_t$
λ_i	ith Lagrange multiplier
$\boldsymbol{\lambda}$	Vector of Lagrange multipliers
$\mu(\mathbf{x})$	Trend function
μ_i	ith coefficient
$\hat{\boldsymbol{\mu}}_m$	Vector containing $\hat{\mu}_0, \cdots, \hat{\mu}_m$
σ_m^2	Variance of $Z(x)$
$\tau_m^2\mathbf{R}$	Prior variance-covariance matrix of $\boldsymbol{\beta}$
$\boldsymbol{\psi}$	Correlation matrix

References

1. Huang, Z.G., Li, Y.L., Chen, Z.H., et al. "Numerical investigations on the drag and aerodynamic characteristics of a hollow projectile", *Acta Armamentarii*, **34**(5), pp. 535-540 (2013).

2. Li, Y.L. and Chen, Z.H. "Aerodynamic characteristics of hollow projectile with a diameter of 30 mm under real conditions", *Aeronautical Computing Technique*, **41**(5), pp. 76-80 (2011).

3. Sasoh, A., Higgins, A.J., Knowlen, C., et al. "Hollow projectile operation in the ram accelerator", *Journal of Propulsion and Power*, **12**, pp. 1183-1186 (1996).

4. Weiss, D. "Field experiments on detonation propelled hollow projectiles", Report W7702-9-R782, Brome Laboratories Inc., Brigham, Quebec, Submitted to Defence R&D Canada-Suffield (2001).

5. Berner, C. and Giraud, M. "Supersonic wind tunnel investigation of a tubular projectile", *11th International Symposium on Ballistics*, Brussels, Belgian, pp. 811-820 (1989).

6. Dupuis, A.D. and Bernier, A. "Free-flight, wind tunnel tests and computational analysis of a spinning tubular projectile at supersonic speeds", *18th International Symposium on Ballistics*, San Antonio, Texas, USA, pp. 70-77 (1999).

7. Ren, D.F., Tan, J.J., and Zhang, J. "Flowfield calculation of hollow projectile using implicit method based on unstructured meshes", *Mechanics in Engineering*, **28**(5), pp. 24-27 (2006).

8. Chen, Y., Liao, Z.Q., Wang, T., et al. "Research on aerodynamic characteristic of hollow projectile with 12.7 mm diameter", *Journal of System Simulation*, **22**(2), pp. 337-339 (2010).

9. Mukesh, R., Lingadurai, K., and Selvakumar, U. "Kriging methodology for surrogate-based airfoil shape optimization", *Arabian Journal for Science and Engineering*, **39**(10), pp. 7363-7373 (2014).

10. Priyadarshi, P., Alam, M., and Saroha, K. "Multidisciplinary multi-objective design optimization of sounding rocket fins", *International Journal of Advances in Engineering Sciences and Applied Mathematics*, **6**(3), pp. 166-182 (2014).

11. Fowler, L. and Rogers, J. "Airframe performance optimization of guided projectiles using design of experiments", *Journal of Spacecraft and Rockets*, **52**(6), pp. 1603-1613 (2015).

12. Wang, R., Zhang, H.J., Wang, G.D., et al. "Multidisciplinary integrated design optimization for an air-breathing air-to-air missile shape", *Acta Aeronautica et Astronautica Sinica*, **37**(1), pp. 207-215 (2016).

13. Wang, G. and Shan, S. "Review of metamodeling techniques in support of engineering design optimization", *Journal of Mechanical Design*, **129**(4), pp. 370-380 (2007).

14. Forrester, A.I.J. and Keane, A.J. "Recent advances in surrogate-based optimization", *Progress in Aerospace Sciences*, **45**(1-3), pp. 50-79 (2009).

15. Viana, F.A.C., Simpson, T.W., Balabanov, V., et al. "Metamodeling in multidisciplinary design optimization: How far have we really come?", *AIAA Journal*, **52**(4), pp. 670-690 (2014).

16. Joseph, V.R., Hung, Y., and Sudjianto, A. "Blind Kriging: a new method for developing Metamodels", *Journal of Mechanical Design*, **130**(3), pp. 1-8 (2008).

17. Antony, J., *Design of Experiments for Engineers and Scientists*, Second Edition, Elsevier Ltd. (2014).

18. Mckay, M.D., Beckman, R.J., and Conover, W.J. "A comparison of three methods for selecting values of input variables in the analysis of output from a computer code", *Technometrics*, **21**(2), pp. 239-245 (1979).

19. Jin, R., Chen, W., and Sudjianto, A. "An efficient algorithm for constructing optimal design of computer experiments", *Journal of Statistical Planning and Inference*, **134**(1), pp. 268-287 (2005).

20. Wang, Z.Y. and Zhou, W.P., *Theory and Method of Exterior Ballistic Design*, Science Press (2004).

21. Wang, Q., Yu, X.G., Qiao, M.J., et al. "Rapid calibration based on SQP algorithm for coordinate frame of localizer", *Journal of Zhejiang University (Engineering Science)*, **51**(2), pp. 319-327 (2017).

Biographies

Qiang Zhao received his MSc from Key Laboratory of Transient Physics, Nanjing University of Science & Technology, China in 2016. Mr. Zhao is in pursuit of his PhD in the same university. His research interests include computational fluid dynamics of supersonic flow, external ballistics and optimal design of projectiles, rockets and missiles.

Zhihua Chen received two PhDs from the New Jersey Institute of Technology, USA in 2001, and Nanjing University of Science & Technology, China in 1997, respectively. Dr. Chen is currently a Professor at the Key Laboratory of Transient Physics, Nanjing University of Science & Technology. His research interests include supersonic and hypersonic flow, external ballistics, and aerodynamic configuration optimization.

Zhengui Huang received his PhD from Key Laboratory of Transient Physics, Nanjing University of Science & Technology, China in 2015. Dr. Huang is currently a Teacher at the Key Laboratory of Transient Physics, Nanjing University of Science & Technology. His research interests include dynamic mesh and multi-bodies separation.

Huanhao Zhang received her PhD from Key Laboratory of Transient Physics, Nanjing University of Science & Technology, China in 2014. Dr. Zhang is currently a Teacher at the Key Laboratory of Transient Physics, Nanjing University of Science & Technology. Her research interests include computational fluid dynamics of supersonic flow and blast system.

Jie Ma received his PhD from Key Laboratory of Transient Physics, Nanjing University of Science & Technology, China in 2016. Dr. Ma is currently a Teacher at School of Mechanical and Power Engineering, Nanjing Tech University. His research interests include aerodynamics and flow separation control.